Orientation-Dependent Electron Transport in a Single Redox Protein

Eduardo Antonio Della Pia,[†,‡] Martin Elliott,[†,*] D. Dafydd Jones,[‡,*] and J. Emyr Macdonald[†]

[†]School of Physics and Astronomy and [‡]School of Biosciences, Cardiff University, Cardiff Wales CF10 3XQ, United Kingdom

ABSTRACT

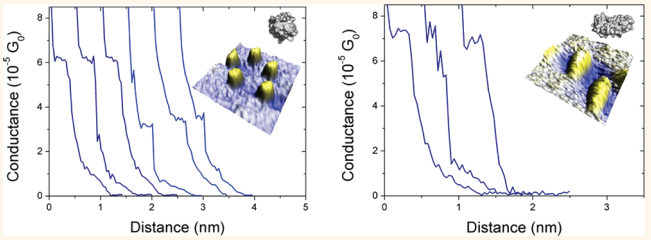

The redox-active protein cytochrome b_{562} has been engineered to introduce pairs of thiol groups in the form of cysteine residues at specified sites. Successful STM imaging of the molecules adsorbed on a gold surface indicated that one thiol group controls the orientation of the molecule and that the protein maintains its native form under the experimental conditions. Stable protein–gold STM tip electrical contact was directly observed to form *via* the second free thiol group in current–voltage and current–distance measurements. Proteins with thiol contacts positioned across the protein's short axis displayed a conductance of $(3.48 \pm 0.05) \times 10^{-5}$ G_0. However proteins with thiol groups placed along the long axis reproducibly yielded two distinct values of $(1.95 \pm 0.03) \times 10^{-5}$ G_0 and $(3.57 \pm 0.11) \times 10^{-5}$ G_0, suggesting that the placement of the asymmetrically located haem within the protein influences electron transfer. In contrast, the unengineered wild-type cytochrome b_{562} had conductance values at least 1 order of magnitude less. Here we show that an electron transfer protein engineered to bind gold surfaces can be controllably oriented and electrically contacted to metallic electrodes, a prerequisite for potential integration into electronic circuits.

KEYWORDS: single-molecule conductance · molecular electronics · nanobioelectronics · scanning tunneling microscopy · cytochrome b_{562} · protein engineering

Electron transfer events are vital in biology, playing a central role in processes such as energy production and catalysis. The primary role of the proteinaceous component in these processes is thought to be binding, organizing, and tuning redox-active cofactors such as heme.[1−4] Although such proteins function at essentially the single molecule level within the cell, most experiments are performed on a molecular ensemble, where variation in individual molecule/environment interactions and events may be obscured.[5,6] Hence there is strong interest in developing methods to probe protein-facilitated electron transport at the single molecule level across a range of fields.[7−9] Measurements of electron transport on single molecules between two contacts[10−16] have been advanced by techniques including electron beam lithography,[17] mechanical break junctions,[18] and Au nanoparticle sandwiches.[19] Among these, scanning tunneling microscopy (STM)-based experiments have allowed current–voltage (I–V) and current–distance (I–z) measurements on single molecules and have been widely used for investigating molecular conductance in a variety of systems. To date, these approaches have been successfully applied to small organic molecules (alkanedithiols,[20−22] conjugated aryl dithiols,[23,24] porphyrins,[25] viologen[26]) but not to more complex molecules such as proteins. Application of these techniques to proteins has been severely hampered by the inability to make direct electrical contact to both electrodes while maintaining the protein's native conformation. Scanning probe measurements have been limited to I–V measurements where there is no intimate contact between the STM tip and the protein molecule or to conducting AFM measurements where a relatively large force, likely to drastically distort the native conformation, is necessary for good electrical contact.[6−8]

Here, we overcome this limitation by engineering thiol contact pairs, through the introduction of cysteine residues, at selected sites on opposing ends of the electron transfer protein cytochrome b_{562} (cyt b_{562}) by site-directed mutagenesis. We demonstrate that the introduced thiol groups are essential for imparting strong protein coupling to both a Au(111) surface and to a gold STM tip electrodes. We also show control of the molecular orientation by preparing two variants with the cysteine residues located at the two ends along the long axis and across the short axis of the ellipsoidally shaped cyt b_{562} and detect

* Address correspondence to martin.elliott@astro.cf.ac.uk, jonesdd@cardiff.ac.uk.

Received for review September 26, 2011 and accepted November 16, 2011.

Published online November 16, 2011
10.1021/nn2036818

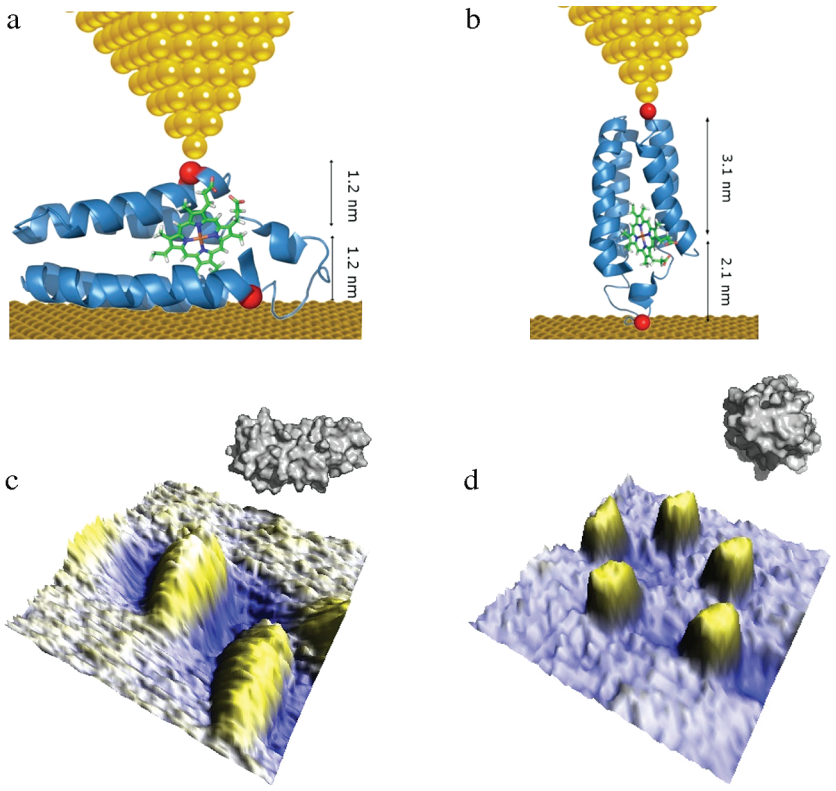

Figure 1. Engineering and imaging of double cysteine mutants cyt b_{562}. The 3D structure of cyt b_{562} variant (a) SH-SA and (b) SH-LA. The relative positions of the amino acid targeted for mutation ((a) Asp5 and Lys104 and (b) Asp21 and Asp50) are highlighted as red spheres, and the heme center is shown in the stick representation and colored green. The gold surface is indicated as yellow spheres. Three-dimensional representation of STM images of (c) SH-SA and (d) SH-LA immobilized on Au(111) after the fifth scan of the same area. The images were acquired at constant I = 0.05 nA and V = −20 mV (size = 12 nm × 12 nm, z-range = 0−1.5 nm). The insets show the surface representations of the (c) side and (d) top views of cyt b_{562} from the X-ray structure.

differences in molecular conductance by $I-V$ and $I-z$ experiments.

Cyt b_{562}, a heme-binding helical bundle electron transfer protein from *Escherichia coli*, has been shown to be suitably robust for repeat STM scans and $I-V$ measurements without unduly influencing the protein's structure and electronic properties.[27,28] As cyt b_{562} does not contain any cysteine residues, thiol groups can be introduced at required positions to define the metal−protein interactions. Replacing residues Asp5 and Lys104 with cysteine residues at diametrically opposite sites across the molecule's short axis generates the cyt b_{562} SH-SA variant (Figure 1a); in this configuration, the protein will have its long axis in the surface plane with the uppermost thiol accessible to the STM tip and its iron center symmetrically positioned ∼1.2 nm from each sulfur atom. The thiol contacts can also be positioned across the protein's long axis by replacing residues Asp21 and Asp50 with cysteine, generating cyt b_{562} SH-LA (Figure 1b). Molecular modeling indicates that SH-LA can anchor metallic surfaces with the iron site being ∼2.0 or ∼3.2 nm distant from the electrodes, depending on which thiol group is bound to the surface. Introduction of cysteines in place of these residues has no effect on the native structure and on the functionality of cyt b_{562}; heme binding and the redox characteristics of the protein are preserved.[27,28]

RESULTS AND DISCUSSION

Robust anchoring of the engineered cyt b_{562} SH-SA and SH-LA variants is demonstrated by the similarity of successive STM images (Supporting Information Figures 1 and 2); by comparison, wild-type cyt b_{562} (containing no thiol groups) is swept away within a few imaging cycles (Supporting Information Figure 3). The observed shape of the cyt b_{562} variants in the STM images was as expected given the overall structure of the protein; cyt b_{562} SH-LA was spherical with SH-SA laterally elongated in comparison (Figure 1c,d). The single cross section profiles were fitted to a Gaussian function, and the measured full width at half-maximum of SH-SA and SH-LA was 5.0 ± 0.6 and 2.3 ± 0.6 nm, respectively, in good agreement with crystallographic data.[29] These results indicate that the proteins retain their native structure upon interaction with the metal surface as unfolded protein will be unlikely to display a defined compact shape on denaturation. It also demonstrates that the introduction of the surface-exposed cysteine plays a vital role for attachment of

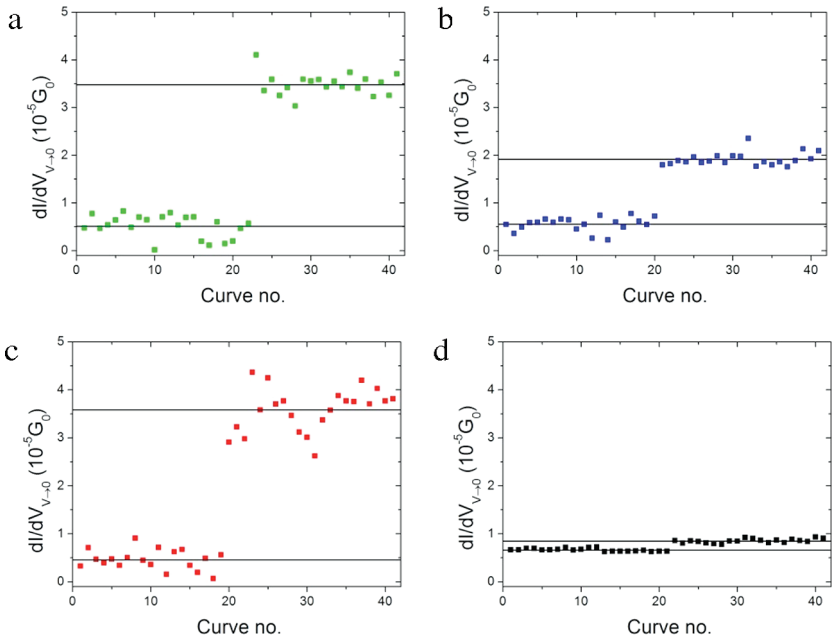

Figure 2. *I*−*V* measurements of cyt b_{562}. Plots of low bias conductance values against the number of the *I*−*V* curve recorded for (a) SH-SA, (b,c) SH-LA, and (d) wild-type cyt b_{562}. The lines are the average of the experimental data (dots).

the molecule in an oriented manner *via* the gold−sulfur bond.

To study the electron transfer properties of the unengineered wild-type and the two cyt b_{562} variants deposited on Au(111) surfaces in their different respective orientations, *I*−*V* measurements were performed. Before and after measuring *I*−*V* curves, molecules were imaged and checked for integrity comparing their lateral dimensions with that of the known molecular structure of cyt b_{562} (Supporting Information Figure 4). Several hundred *I*−*V* curves were recorded in a low bias range (−0.75 V, +0.75 V) at a rate of 20 V/s without re-establishing the feedback system and fitted to a third-order polynomial function:

$$I = AV + BV^3 \quad (1)$$

where *A* is the low bias conductance (*i.e.*, the first derivative of the current with respect to voltage near 0 ($dI/dV_{V\to0}$)) and *B* is a coefficient that describes the nonlinearity of the *I*−*V* curve (second- and higher-order polynomial coefficients were insignificant at the small bias voltages used in the experiments). The evaluated low bias conductance was plotted against the number of the corresponding recorded curve to display any changes in conductance, which may arise due to changes in tunneling distance or tunneling barrier.

With the system out of feedback, in most cases, just a slow increase or decrease in conductance over time was observed as the tip drifted either toward or away from the sample (Supporting Information Figure 5). However, sudden characteristic changes were observed in 15−20% of the *I*−*V* traces when probing cyt b_{562} SH-SA and SH-LA (Supporting Information Figure 6). These differences are revealed by jumps in low bias conductance against scan number and are attributed to the binding of the free thiol to the STM tip (Figure 2). Conductance jumps for SH-SA (Figure 2a) and SH-LA (Figure 2b,c) are $\sim(1-3) \times 10^{-5}$ G_0 (G_0 = 77.4 μS). Similar events have been reported in current measured as a function of time (*I*−*t*) experiments conducted with alkanedithiols[26] and short DNA molecules functionalized with two thiol groups.[30] *I*−*V* curves were also recorded for the wild-type cyt b_{562} (Supporting Information Figure 6a). Although jumps in conductance were observed (Figure 2d), they were an order of magnitude lower ($\sim2 \times 10^{-6}$ G_0) than the engineered cyt b_{562} variants, indicating that in the absence of thiol groups the junction resistance increased and that only poor non-optimal protein−electrode contact was possible. *I*−*V* control experiments were performed on bare Au(111) electrodes (Supporting Information Figure 7). These showed little variation in the observed conductance over time (Supporting Information Figure 7a); the measured current was similar to the one recorded when the proteins were adsorbed on the Au(111) surface before a characteristic step-change in conductance. In a few instances (~10%), the measured current saturated the amplifier, indicating that the tip was in contact with the gold surface (Supporting Information Figure 7b).

The low bias conductance values measured for SH-SA ($(3.48 \pm 0.05) \times 10^{-5}$ G_0, Figure 2b) were more stable over time than SH-LA possibly because of more robust binding of the protein sulfur group to the tip. In addition, measurements with SH-LA (Figure 2c,d) had two distinct conductance jumps ($(1.95 \pm 0.03) \times 10^{-5}$ G_0 and $(3.57 \pm 0.11) \times 10^{-5}$ G_0). The two observed

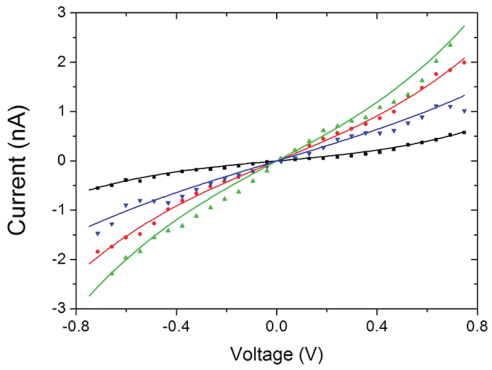

Figure 3. Example of fitting curve (lines) of experimental *I*−*V* curves (dots) for (green) SH-SA, (red and blue) SH-LA, and (black) wild-type cyt b_{562} using eq 1 in the main text. For clarity, only 1 from every 10 experimental data points of the *I*−*V* curves observed after a jump in $dI/dV_{V\to 0}$ value is plotted. The STM feedback loop (set point bias voltage 0.1 V, tunneling current 50 pA) was disengaged, and the *I*−*V* characteristics were recorded.

values were reproducibly associated with distinct SH-LA proteins adsorbed on the Au(111) surface. The most likely explanation of the two observed conductance values is that they relate to two different orientations of the protein with respect to the gold surface, resulting from immobilization *via* the thiol either at residue 21 or at residue 50. The SH-LA protein binding the Au surface through the cysteine at position 21 has the metal center closer to the scanning tip (~2.0 nm) than the protein binding through the cysteine at position 50 (~3.2 nm) (Figure 1b). This asymmetry will affect the relative coupling of the iron moiety to the tip and metal surface. In turn, this will affect the broadening of the highest occupied molecular orbital (HOMO) and the lowest unoccupied molecular orbital (LUMO) electronic levels of the molecule due to the interaction of the redox center with the electrodes[31] as a result of the different geometry of the Au tip and the Au(111) substrate.[32−35] This is supported by experiments and theoretical calculations performed with alkanedithiols molecules, where it has been shown that the electronic coupling between the molecules and a flat Au(111) surface is different to that with a rough gold surface.[33−36] The asymmetry will also give rise to different interface dipoles at the metal surface, which could contribute to differences in the measured current for the two molecular orientations.

Recording *I*−*V* curves repeatedly over time, as presented above, is an extension of *I*−*t* experiments where the current is simply recorded at a fixed bias as a function of time.[26] Our experimental setup enables us not only to monitor jumps in current due to the contact between molecule and tip but also to analyze conduction mechanisms through investigation of the *I*−*V* curves (Figure 3). The third-order polynomial function (eq 1) fits well to the experimental *I*−*V* curves over the full bias range. The *B* parameter (eq 1), which determines the curvature of the *I*−*V* curves, can be interpreted in a tunneling barrier model in terms of the width and the height of the tunneling barrier,[37] and its value suggests that the effective barrier height (φ_0) for the wild-type protein is about two times larger than that for the double cysteine mutants. This result supports our hypothesis of a good thiol−Au contact for the proteins containing the thiol moieties. Lack of knowledge of the contact area for electronic transport between the proteins and the electrodes (different from the nominal geometric contact area) prevents extracting absolute values for barrier height. An alternative, and physically more accurate, treatment of molecular conduction in cyt b_{562} is to invoke the stronger coupling of the tunneling pathway through the heme, mediated by the covalent Au−thiol bond at each end.[28,31,32] This coupling would increase the conductance in either the case of coherent molecular tunneling or the case of Marcus-like electron transfer.

We have also performed *I*−*z* experiments that require the STM tip to be brought into contact with the molecule and retracted at constant bias, while measuring the current flow through the protein trapped in the junction. For the *I*−*z* traces recorded with the STM tip placed on the SH-SA (Figure 4a) or SH-LA molecules (Figure 4b,c), exponential decay of current with distance was initially measured and then plateaus were observed. The measured current remains fairly constant, indicating that the Au−S bond is intact, but as the tip is retracted to the point at which contact is broken, the current suddenly drops.[23−26] The plateaus in the *I*−*z* traces of SH-SA and SH-LA molecules suggest conduction through a good electronic contact between the tip and the free thiol of the protein; in contrast, a relatively rapid exponential decay of current without plateaus within the stretched distance is observed for wild-type cyt b_{562} (Figure 4d).

Low STM lateral drift (~3 pm/s) allowed stable and reliable *I*−*z* measurements of single proteins. Measurement of a large number of molecular junctions allowed robust statistical analysis to be performed. Raw current data of the curves displaying current plateaus were divided by bias voltage (100 mV) and the calculated conductance converted to histograms using 10 bins/nS (Figure 4e−h). The conductance histograms for SH-SA (Figure 4e) and SH-LA (Figure 4f,g) displayed several distinct peaks, unlike the wild-type cyt b_{562} (Figure 4h). The SH-SA variant was found to be more conductive ($(6.5 \pm 0.1) \times 10^{-5}\ G_0$) than the SH-LA ($(3.45 \pm 0.05) \times 10^{-5}\ G_0$ and $(5.20 \pm 0.03) \times 10^{-5}\ G_0$), which may be due to the different distance between the electrodes and the heme redox center (Figure 1). As already noted for the *I*−*V* experiments, the SH-LA have two different conductance values that are related to two separate classes of molecules (indicated with A and B in Figure 4b,c). The calculated conductance values are in good agreement with the low bias conductance found in the earlier *I*−*V* experiments involving a nominally

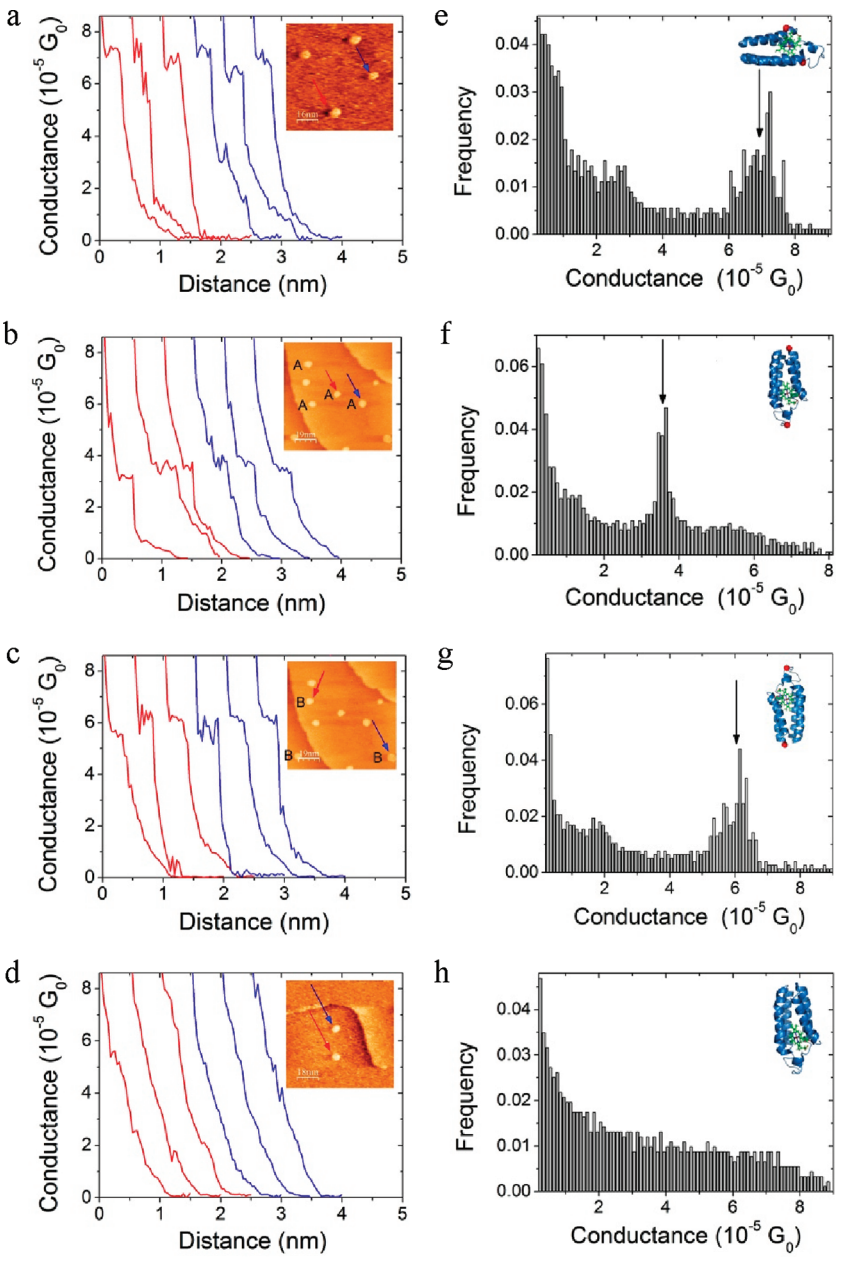

Figure 4. *I*–*z* measurements of cyt b_{562}. (a–d) Conductance against distance curves of (a) SH-SA, (b,c) SH-LA, and (d) wild-type for the specific molecules labeled with red and blue arrows in the insets. For clarity, the conductance traces are displaced along the *x* axis. (e–h) Conductance histograms corresponding to (a–d). In (a) and (d), the displayed curves are typical of those for all molecules studied. In contrast, the SH-LA molecules (b,c) showed two distinct behaviors: the molecules labeled A repeatedly gave conductance curves similar to those in (b) and corresponding histograms as in (f), and those labeled B gave curves as in (c) and histograms as in (g). The orientation of the SH-LA molecule cartoon in (f) and (g) is not representative of their actual orientation.

static tip. All observations from the *I*–*z* experiments are consistent with the *I*–*V* measurements and support our contention that the surface-exposed cysteines represent an ideal way for contacting the protein with metal electrodes.

CONCLUSIONS

In summary, we report a detailed analysis of the conductivity properties of two engineered cyt b_{562} variants adsorbed onto Au(111) by a combination of STM, *I*–*V*, and *I*–*z* techniques. The two double cysteine cyt b_{562} variants present thiols at opposite ends of the protein and allow stable binding to the gold surface in defined orientations. While STM imaging revealed that the presence of a thiol is vital for protein binding to a metal electrode, the *I*–*V* and the *I*–*z* experiments showed that a second free thiol provides a means for enhancing electrical contacts with a second metal surface. *I*–*V* curves recorded over time indicated that both variants were coupled tightly to the electrodes with conduction larger than the wild-type cyt b_{562} that lacks thiol groups. The *I*–*z* method has been applied

for the first time to proteins and allows the study of electronic properties of a single molecule while controlling the tip−sample distance. The measured conductivity was shown to depend on the orientation of the proteins and the position of the heme relative to the two electrodes. The conduction mechanism of biomolecules is still debated; our work demonstrates that, when engineered appropriately, a redox protein can bridge two electrodes allowing electronic properties at a single molecule level to be probed.

EXPERIMENTAL SECTION

STM, *I*−*V*, and *I*−*z* experiments were performed in air at room temperature using a home-built instrument. The system is based on two small, concentric cylindrical piezotubes (7.0 mm and 11.2 mm in diameter) that are used for the coarse approach and to scan in the *z*-direction (external piezo) and for scanning the sample in the *x* and *y* plane (internal piezo). The special design makes the STM very stable in terms of lateral drift and insensitive to mechanical vibration. The system is equipped with an *I*−*V* converter with a sensitivity of 1 nA/V.

STM tips used throughout the experiments were mechanically cut from Au(99.9%) 0.25 mm diameter wires (Goodfellow, UK). Au(111) bead single crystal substrates were cleaned by electropolishing in 1 M H_2SO_4 and washed with 0.1 M HCl and water. The samples were annealed for 8 h at 880 °C in order to obtain recrystallized terraces. The samples were then incubated with 5 μM protein solution (10 mM phosphate buffer pH 6.2 and 50 mM NaCl) at room temperature for 5 min. Samples were rinsed with ultrapure water (resistivity 18.2 MΩ·cm) to remove the weakly bound proteins and the buffer excess, gently dried with a flow of nitrogen and then imaged. Wild-type, SH-SA, and SH-LA cyt b_{562} proteins used in the present experiments were expressed, purified, and analyzed by UV−visible spectroscopy as described in previous papers.[26,27]

I−*V* and *I*−*z* measurements were performed in air after scanning the substrate and checking for tip integrity. Once single protein resolution was achieved and thermal drift had stabilized (few pm/s), the gold tip was placed above a protein at a tunneling resistance of 2 GΩ (50 pA, 0.1 V with the sample held at a negative potential). In the *I*−*V* experiments, the feedback loop was then disengaged and the current was recorded with the voltage ramping between −0.75 and +0.75 V for typically 20 s (10 curves measured per second). In the *I*−*z* experiments, the tip was moved toward the sample by 2 nm. After disengaging the feedback loop, the tip was moved away from the sample at a rate of 20 nm/s and the current recorded as function of tip distance. In order to be able to perform a meaningful statistical analysis, the measurements were performed on a large number of proteins deposited on different Au(111) surfaces with various gold tips. The proteins were checked for integrity and stable binding after collecting each set of data. Only *I*−*V* and *I*−*z* curves where the proteins' dimensions were not modified by the tip during the experiments were included in the analysis (Supporting Information Figures 4 and 8).

Acknowledgment. E.A.D.P. was supported by a Cardiff University Richard Whipp Interdisciplinary Research studentship. This work was supported by BBRSC (Grant BB/E001084 to D.D.J.) and EPSRC (EP/D076072/1 to J.E.M. and M.E.).

Supporting Information Available: STM images and *I*−*V* curves of SH-SA, SH-LA, and wild-type cyt b_{562}. This material is available free of charge *via* the Internet at http://pubs.acs.org.

REFERENCES AND NOTES

1. Edwards, W. R.; Williams, A. J.; Morris, J. L.; Baldwin, A. J.; Allemann, R. K.; Jones, D. D. Regulation of β-Lactamase Activity by Remote Binding of Heme: Functional Coupling of Unrelated Proteins through Domain Insertion. *Biochemistry* **2010**, *49*, 6541–6549.
2. Edwards, W. R.; Busse, K.; Allemann, R. K.; Jones, D. D. Linking the Functions of Unrelated Proteins Using a Novel Directed Evolution Domain Insertion Method. *Nucleic Acids Res.* **2008**, *36*, e78.
3. Jones, D. D.; Barker, P. D. Controlling Self-Assembly by Linking Protein Folding, DNA Binding, and the Redox Chemistry of Heme. *Angew. Chem., Int. Ed.* **2005**, *44*, 6337–6341.
4. Jones, D. D.; Barker, P. D. Design and Characterisation of an Artificial DNA-Binding Cytochrome. *ChemBioChem* **2004**, *5*, 964–971.
5. Hook, F.; Kasemo, B.; Grunze, M.; Zauscher, S. Quantitative Biological Surface Science: Challenges and Recent Advances. *ACS Nano* **2008**, *2*, 2428–2436.
6. Ron, I.; Sepunaru, L.; Itzhakov, S.; Belenkova, T.; Friedman, N.; Pecht, I.; Sheves, M.; Cahen, D. Proteins as Electronic Materials: Electron Transport through Solid-State Protein Monolayer Junctions. *J. Am. Chem. Soc.* **2010**, *132*, 4131–4140.
7. Claridge, S. A.; Schwartz, J. J.; Weiss, P. S. Electrons, Photons, and Force: Quantitative Single-Molecule Measurements from Physics to Biology. *ACS Nano* **2011**, *5*, 693–729.
8. Galipeau, K. K.; Nanayakkara, S.; O'Brian, P. A.; Nikiforov, M.; Discher, B. M.; Bonnell, D. A. Direct Probe of Molecular Polarization in *De Novo* Protein−Electrode Interfaces. *ACS Nano* **2011**, *5*, 4835–4842.
9. Artes, J. M.; Diez-Perez, I.; Sanz, F.; Gorostiza, P. Direct Measurement of Electron Transfer Distance Decay Constants of Single Redox Proteins by Electrochemical Tunneling Spectroscopy. *ACS Nano* **2011**, *5*, 2060–2066.
10. Song, H.; Reed, M. A.; Lee, T. Single-Molecule Devices: Single Molecule Electronic Devices. *Adv. Mater.* **2011**, *23*, 1583–1608.
11. Wang, Y.; Mirkin, C. A.; Park, S.-J. Nanofabrication beyond Electronics. *ACS Nano* **2009**, *3*, 1049–1056.
12. Hipps, K. W. Molecular Electronics: It's All about Contacts. *Science* **2001**, *294*, 536–537.
13. Tao, N. J. Electron Transport in Molecular Junctions. *Nat. Nanotechnol.* **2006**, *1*, 173–181.
14. Ashwell, G. J.; Phillips, L. J.; Robinson, B. J.; Urasinska-Wojcik, B.; Lambert, C. J.; Grace, I. M.; Bryce, M. R.; Jitchati, R.; Tavasli, M.; Cox, T. I.; *et al.* Molecular Bridging of Silicon Nanogaps. *ACS Nano* **2010**, *4*, 7401–7406.
15. Chen, F.; Hihath, J.; Huang, Z.; Li, X.; Tao, N. J. Measurement of Single-Molecule Conductance. *Annu. Rev. Phys. Chem.* **2007**, *58*, 535–564.
16. Nichols, R. J.; Haiss, W.; Higgins, S. J.; Leary, E.; Martin, S.; Bethell, D. The Experimental Determination of the Conductance of Single Molecules. *Phys. Chem. Chem. Phys.* **2010**, *12*, 2801–2815.
17. Steinmann, P.; Weaver, J. M. R. Nanometer-Scale Gaps between Metallic Electrodes Fabricated Using a Statistical Alignment Technique. *Appl. Phys. Lett.* **2005**, *86*, 1–3.
18. Ulgut, B.; Abruna, H. D. Electron Transfer through Molecules and Assemblies at Electrode Surfaces. *Chem. Rev.* **2008**, *108*, 2721–2736.
19. Haick, H.; Cahen, D. Making Contact: Connecting Molecules Electrically to the Macroscopic World. *Prog. Surf. Sci.* **2008**, *83*, 217–261.
20. Cui, X. D.; Primak, A.; Zarate, X.; Tomfohr, J.; Sankey, O. F.; Moore, A. L.; Moore, T. A.; Gust, D.; Harris, G.; Lindsay, S. M. Reproducible Measurement of Single-Molecule Conductivity. *Science* **2001**, *294*, 571–574.
21. Bennett, N.; Xu, G.; Esdaile, L. J.; Anderson, H. L.; MacDonald, J. E.; Elliott, M. Transition Voltage Spectroscopy of Porphyrin Molecular Wires. *Small* **2010**, *6*, 2604–2611.

22. Kim, Y.; Hellmuth, T. J.; Borkle, M.; Pauly, F.; Scheer, E. Characteristics of Amine-Ended and Thiol-Ended Alkane Single-Molecule Junctions Revealed by Inelastic Electron Tunneling Spectroscopy. *ACS Nano* **2011**, *5*, 4104–4111.
23. Haiss, W.; Wang, C.; Grace, I.; Batsanov, A. S.; Schiffrin, D. J.; Higgins, S. J.; Bryce, M. R.; Lambert, C. J.; Nichols, R. J. Precision Control of Single-Molecule Electrical Junctions. *Nat. Mater.* **2006**, *5*, 995–1002.
24. Xiao, X.; Xu, B.; Tao, N. J. Measurement of Single Molecule Conductance: Benzenedithiol and Benzenedimethanethiol. *Nano Lett.* **2004**, *4*, 267–271.
25. Sedghi, G.; Sawada, K.; Esdaile, L. J.; Hoffmann, M.; Anderson, H. L.; Bethell, D.; Haiss, W.; Higgins, S. J.; Nichols, R. J. Single Molecule Conductance of Porphyrin Wires with Ultralow Attenuation. *J. Am. Chem. Soc.* **2008**, *130*, 8582–8583.
26. Haiss, W.; Nichols, R. J.; Van Zalinge, H.; Higgins, S. J.; Bethell, D.; Schiffrin, D. J. Measurement of Single Molecule Conductivity Using the Spontaneous Formation of Molecular Wires. *Phys. Chem. Chem. Phys.* **2004**, *6*, 4330–4337.
27. Della Pia E. A., Macdonald J. E., Elliott M., Jones D. D. Direct Binding of an Electron Transfer Protein for Single Molecule Electron Measurements *Small*, submitted for publication.
28. Della Pia, E. A.; Chi, Q.; Jones, D. D.; Macdonald, J. E.; Ulstrup, J.; Elliott, M. Single-Molecule Mapping of Long-Range Electron Transport for a Cytochrome b_{562} Variant. *Nano Lett.* **2011**, *11*, 176–182.
29. Hamada, K.; Bethge, P. H.; Mathews, F. S. Refined Structure of Cytochrome b_{562} from *Escherichia coli* at 1.4 Å Resolution. *J. Mol. Biol.* **1995**, *247*, 947–962.
30. Van Zalinge, H.; Schiffrin, D. J.; Bates, A. D.; Haiss, W.; Ulstrup, J.; Nichols, R. J. Single-Molecule Conductance Measurements of Single- and Double-Stranded DNA Oligonucleotides. *ChemPhysChem* **2006**, *7*, 94–98.
31. Pobelov, I. V.; Li, Z.; Wandlowski, T. Electrolyte Gating in Redox-Active Tunneling Junctions-An Electrochemical STM Approach. *J. Am. Chem. Soc.* **2008**, *130*, 16045–16054.
32. Li, C.; Pobelov, I.; Wandlowski, T.; Bagrets, A.; Arnold, A.; Evers, F. Charge Transport in Single Au|Alkanedithiol|Au Junctions: Coordination Geometries and Conformational Degrees of Freedom. *J. Am. Chem. Soc.* **2008**, *130*, 318–326.
33. Sen, A.; Kaun, C. C. Effect of Electrode Orientations on Charge Transport in Alkanedithiol Single-Molecule Junctions. *ACS Nano* **2010**, *4*, 6404–6408.
34. Li, X.; He, J.; Hihath, J.; Xu, B.; Lindsay, S. M.; Tao, N. Conductance of Single Alkanedithiols: Conduction Mechanism and Effect of Molecule−Electrode Contacts. *J. Am. Chem. Soc.* **2006**, *128*, 2135–2141.
35. Li-Li, L.; Wang, C.-K.; Luo, Y. Inelastic Electron Tunneling Spectroscopy of Gold−Benzenedithiol−Gold Junctions: Accurate Determination of Molecular Conformation. *ACS Nano* **2011**, *5*, 2257–2263.
36. Haiss, W.; Martin, S.; Leary, E.; Van Zalinge, H.; Higgins, S. J.; Bouffier, L.; Nichols, R. J. Impact of Junction Formation Method and Surface Roughness on Single Molecule Conductance. *J. Phys. Chem. C* **2009**, *113*, 5823–5833.
37. Vilan, A. Analyzing Molecular Current−Voltage Characteristics with the Simmons Tunneling Model: Scaling and Linearization. *J. Phys. Chem. C* **2007**, *111*, 4431–4444.